Soft Matter

COMMUNICATION

View Article Online
View Journal | View Issue

Cite this: *Soft Matter*, 2024, **20**, 8012

Received 5th August 2024,
Accepted 29th September 2024

DOI: 10.1039/d4sm00943f

rsc.li/soft-matter-journal

Zombie diatoms: acoustically powered diatom frustule bio-templated microswimmers†

Mehmed C. Ozkan, ‡[a] Jeffrey M. McNeill‡[b] and Thomas E. Mallouk *[a]

Frustules, or the silica based cell walls of diatomaceous algae *Aulacoseira granulata*, provide large numbers of reliably cylindrical microstructures with an inner cavity and surface chemistry suitable for constructing bubble-based, acoustically-powered micro-swimmers. In this way, microswimmers can be made in a scalable, accessible and low-cost manner, enabling studies of their individual and collective behavior as active colloids.

Microswimmers are artificial micro- to nanoscale objects that are designed to respond to one or a combination of energy sources such as light, electric or magnetic fields, chemical fuels, or ultrasound to produce motion.[1–4] These swimmers can attain relatively high speeds and are capable of manipulating particles of similar size.[5] Because of these capabilities, they are potential tools for drug delivery and diagnostics, as model systems in the study of active matter, and as analogues to biological 'pushers' such as flagellar bacteria.[6] These promising properties and applications are unfortunately overshadowed by the fact that the swimmers typically lack scalable synthetic methods that would enable studies at densities similar to those of bacterial colonies or dense colloidal suspensions.

While emulsion-based methods exist for synthesizing Janus particle swimmers in large quantities,[7] these types of swimmers fall short in their biocompatibility or ease of operation. Chemically-powered Janus swimmers typically require the use of cytotoxic fuels and weakly ionic environments.[4] While swimmers propelled by magnetic and electric fields have shown promise in biological environments and provide evidence of complex behavior,[8,9] these swimmers are not autonomous and must be externally controlled at all times.

Microstructures powered by an external acoustic source have variety of ways in which they can convert acoustic excitation into movement. The modes of particle manipulation that can be achieved in acoustofluidic systems is both complex and precise.[10,11] Previous examples of swimmers that use acoustic power include helical microrobots inspired by *Spirochete* bacteria,[12] artificial ciliary bands inspired by starfish,[13] controllable and self-assembling lipid-microbubbles that navigate brain vasculature[14] and bullet-shaped surface-lipping swimmers that can be steered by an external magnetic field.[15] Microswimmers propelled by an acoustically-actuated bubble improve upon the issues that limit chemically powered swimmers and allow one to more easily study swimming and collective effects at the micron length scale.[16] They are fast, efficient, and can work in combination with chemical, flow, and magnetic fields for steering. They are propelled by an intrinsic directional autonomous propulsion source (the bubble), coupled to the external acoustic field only through resonance with an ultrasound transducer. The propulsion force arises from acoustic streaming, as analyzed in detail in previous papers on bubble based microswimmers.[1,17] Hence, the only requirement to construct a bubble-based acoustically powered microswimmer is a structure that can maintain a gas microbubble when immersed in water. As a result, the swimmer can theoretically be very simple in geometry. A simple, scalable swimmer design is needed to study these interactions at higher number densities in a variety of environments. This could potentially expand the implementation of acoustofluidics in biomedical applications[11,18,19] and beyond.

Diatoms (Bacillariophyta) are photosynthetic microalgae responsible for much of the oxygen we breathe. Their cell walls are composed of hydrated mesoporous silica[20] and are referred to as frustules. Although crystallographically amorphous, the frustules have highly regular nano to microscale features in the form of pores, ridges and tubular structures.[21] With very many species of sizes ranging from microns to millimeters, diatoms provide a rich variety of micro-scale morphologies, and within a single species these features are faithfully replicated. An earlier

[a] *Department of Chemistry, 231 S. 34 Street, Philadelphia, PA 19104, USA. E-mail: mallouk@sas.upenn.edu*
[b] *Department of Chemistry, 3000 Broadway, Havemeyer Hall, New York, NY 10027, USA. E-mail: jm5750@columbia.edu*

† Electronic supplementary information (ESI) available: Experimental and computational methods, results of numerical simulations, optical images and videos (xx pp). See DOI: https://doi.org/10.1039/d4sm00943f

‡ These authors contributed equally to this work.

report of frustules propelled by catalytic hydrogen peroxide decomposition suggested that they possess surface features that could trap gas bubbles.[22] However, the wide variety of geometries present in the diatomaceous earth samples used in that work precluded a systematic study of acoustically-actuated autonomous propulsion.

Here we report the use of the frustules harvested from a live diatom strain of *Aulacoseira granulata* to make acoustically powered, autonomously propelled microswimmers. We isolated the cylindrical frustules by breaking up the filamentous colonies into uniform short segments. Vapor coating with a hydrophobic silane activated the frustules to trap a gas bubble in aqueous media. These "zombie" diatoms replicate the previously reported swimming behavior of bubble based acoustic swimmers.[1] Due to the inherent genetic variety available in nature and the scalability of the procedure, we propose this as a method to rapidly and easily probe a wider variety of morphologies and bulk active matter behavior.

We cultivated the diatoms from a commercially available culture and diatom growth media in simple glass jars and converted them to bubble-based swimmers using the process flow sketched in Fig. 1. Acoustically powered swimming was studied by optical microscopy with a PZT transducer coupled to a silicon wafer. We characterized bulk swimmer motion as a function of acoustic frequency by taking the pixel difference between two frames in a video synced to a sweeping sinusoidal function generator. We present descriptors for the swimming behavior such as example particle trajectories and mean square displacements (MSD) measured and calculated directly through automated single particle tracking and MSD analysis software (see ESI† Section S3 for full experimental details).

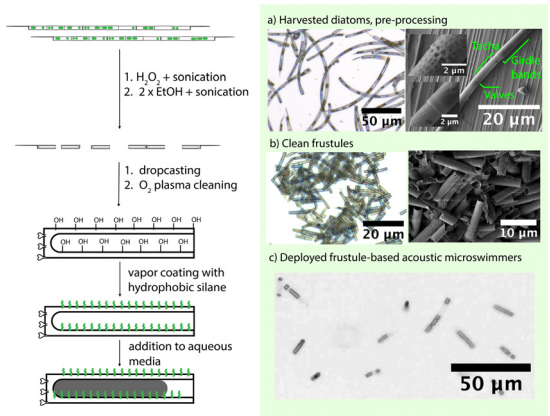

Fig. 1 Schematic overview of the microswimmer fabrication from living filamentous diatom colonies to final cylindrical form. (a) Optical and SEM micrographs of unprocessed *Aulacoseira g.* samples, illustrating the two distinct links that segments of the diatoms have: a dove-tail-like connection between techa of adjacent diatom cells and an interfacial fit between the thin rings of silica that connect the techa within a cell's frustule (Girdle bands), (b) frustules after processing with hydrogen peroxide, ethanol and sonication, (c) frustules coated in hydrophobic silane submerged in an aqueous medium inside the experimental chamber. The darker color cylinders are the air-bubbles encased within the lighter-gray cylindrical frustules.

Diatoms were cultivated according to the process described in the ESI.† Aliquots of the colony were dried on substrates and imaged by optical microscopy and SEM, which revealed the anatomy shown in Fig. 1a. The cylindrical segments of the frustules are connected by a what resembles dove-tail-like and interface fits with organic content from the cytoplasm visible inside. This suggests that a combination of mechanical force and chemical bleaching/washing can break apart and clean the diatoms. As a result, we found that sequential sonication in hydrogen peroxide and ethanol yielded clean and singular units of cylindrical frustules (Fig. 2). We then drop-cast the frustules on a clean silicon wafer and dry them, followed by the vapor coating of the frustules with 1*H*,1*H*,2*H*,2*H*-perfluorooctyltrichlorosilane (97%) to make them hydrophobic, the details of which are highlighted in Section S2 of the ESI,† Fig. S3.

The frustules were deployed in aqueous media using the well setup shown in Fig. S7 (see ESI†). We placed ~4.5 µL of nanopure water containing 0.1 wt% sodium dodecyl sulfate (SDS) on the hydrophobic frustules and repeatedly aspirated and expelled the liquid in the micropipette. This suspended the swimmers in solution and enabled transfer to the experimental chamber and a bubble of air was trapped inside them as shown in Fig. 3. The surfactant was essential as it enabled the swimmers to resist aggregation and freely slide onto the surface of the substrate and the glass-slide cover. The optimized 0.1 wt% SDS amount represented a compromise between the mobility of individual swimmers and the longevity of the bubble to achieve minutes to hours of experiment time at the acoustic fields. Too much surfactant can cause the bubble to pop prematurely as it forms a low energy interface between the hydrophobic chains and the aqueous media. With this setup, we could observe the swimmers move in a pseudo-planar fashion using an optical microscope while varying the frequency and power of the acoustic power source. The microswimmers are predicted to have a fundamental resonant

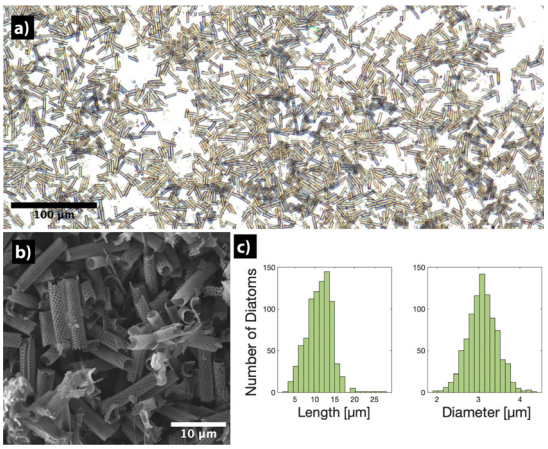

Fig. 2 (a) Optical microscopy of the processed, separated cylindrical segments of the diatoms, now in the form of shorter, uniform cylindrical frustules that can be used as a scaffold for the microswimmers, (b) SEM image of the clean frustules (c) histograms of the lengths and diameters of the processed diatom frustules.

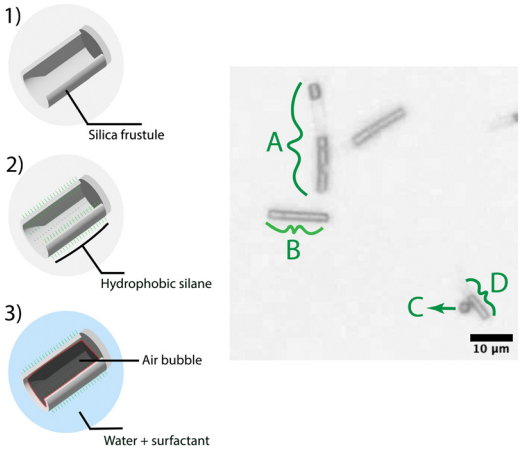

Fig. 3 Images of swimmers. The darker regions are the air bubbles trapped inside the lighter gray cylindrical cavities. The clean silica-based frustule (1), after coating with the hydrophobic silane (2) has a trapped air bubble in the cavity, which persists when the swimmer is placed in aqueous media (3) (A) two cylinders still attached, (B) two longer cylinders attached, partial bubble in one, (D) small singular cylinder.

frequency at which they are most active, as well as many potential radial and axial modes. The piezoelectric transducer itself also has many resonant modes at which it produces a higher acoustic pressure. We expect the frequency response of the swimmers at a certain peak-to-peak sinusoidal voltage provided to the transducer to be modulated by these nonlinear responses to frequency changes. We can also expect that coupling to the silicon wafer, as well as the experimental cavity itself has its own resonant modes, further increasing the complexity. At this stage, it was important to develop a rapid and computationally simple method to map swimmer activity to frequency.

To do this, we adapted an algorithm[23] that averages frames around a frame of interest in a video and takes the difference between the image and the frame. A threshold was introduced to eliminate pixel differences that occurred due to noise in the video. The total count of pixels that are different functions as a measure of the activity per frame. We could then sync this video to cycles of a frequency sweep function on the signal generator and plot this activity as a function of frequency. Doing this for many cycles, automatically parsing each cycle and adding the activities revealed a replicable and quick way to map bulk level activity of swimmers as a response to changing frequency.

As seen in Fig. 4, the swimmer activity was the highest at around 1 MHz, particularly 1.04 MHz, which was close to the expected primary resonance frequency of the PZT transducer (STEINER & MARTINS, INC. SMD15T21R111WL disc transducer, 1 MHz ± 3%). Thus, in these experiments, the transducer's vibrational modes appear to be the dominating factor in determining the swimmer's activity at a given frequency.

As expected, the average mean square displacement (MSD) of particles was found to increase with voltage (Fig. S8 see ESI,† and Video S1: trajectories with varying voltage). We note that at high voltages, forces caused by the presence of nodes and anti-nodes in surface modes of the transducer-wafer cause swimmers to

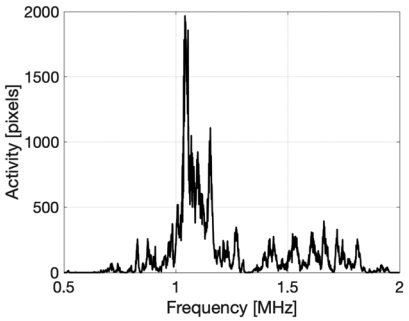

Fig. 4 Frequency response of the microswimmers. Bulk motion was characterized by calculating the difference between frames and registering pixels over a threshold value. Frequency sweep of a sinusoidal wave from 0.5 MHz to 2 Mhz over 80 seconds, at 0.5 Vpp.

aggregate in geometric patterns expected for 2D acoustic standing waves. Increasing the signal power to above 5 Vpp drastically reduced the bubble lifetime. With this in mind, we were able to observe the swimmers move at 1.04 MHz, with the signal generator set to a peak-to-peak 0.5 V sinusoidal wave, which was previously found to be a good operation voltage for the swimmers produced by lithography.[17] We then recorded several minutes of activity at a time and extracted trajectories of individual particles using the Mosaic[24] plugin of the open source image processing software Fiji.[25] The MSD and related analysis was performed using @MSDAnalyzer[26] plugin and MATLAB.[27] The slope of the log–log of an MSD *vs.* time plot provides of a quantitative metric of the type of powered movement. If the slope of this plot α is below 1, the swimmers are sub-diffusive, if α is between 1 and 2 the swimmers are super-diffusive. The data, subjected to a *t*-test ($p < 0.05$), showed that at 0.5 Vpp the swimmers were significantly super-diffusive, and at 0 Vpp significantly sub-diffusive as they were mostly stationary (Fig. 5).

Single particle tracks (Fig. 6) greatly resembled the non-steered/low surface attraction scenarios of swimmers made by lithography and demonstrated similar speeds, suggesting that bubble-powered diatom frustules extend the same concept to a bio-templated and scalable form.[17]

Though we observed several complex and evolving types of trajectories (see ESI† Video S2: complex trajectories close-up) and behaviors due to asymmetries of the frustules, we mainly

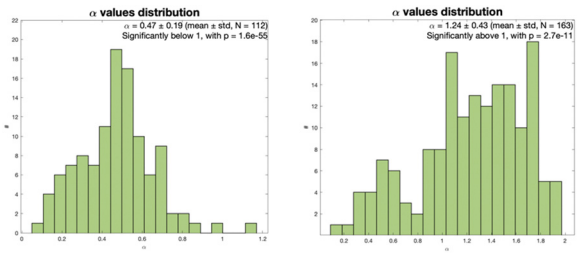

Fig. 5 Alpha α values of swimmers subjected to no acoustic power *vs.* 0.5 Vpp. No power results in stationary/sub-diffusive behavior whereas powering causes statistically significant super-diffusive swimming in the bulk.

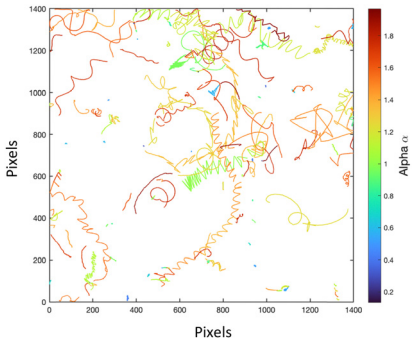

Fig. 6 Tracks of an example selection of swimmers subjected to a sinusoidal sound wave at 1.04 MHz, 0.5 Vpp.

saw the behavior summarized in Fig. 7. These behaviors are a result of a combination of streaming propulsion, which propels the microswimmers forward, and the secondary Bjerknes force, which causes attraction towards other bubbles and images of their own bubbles on acoustically reflective surfaces such as the glass slide and the silicon wafer that forms the chamber. We can determine the magnitude of the propulsive force by using the Stokes drag force on a microcylinder, described by $f = 2\pi\mu Lv/(\ln(L/R) - 0.72)$, where μ is the dynamic viscosity of water, L is the length of the cylindrical rod, R is its radius, and v is the velocity of the swimmers.[28] From the average of six representative tracks in ESI,† Video S2 that are sufficiently planar and close to the glass plane, we found that the swimmers generate apparent streaming forces on the order of 0.78 pN (std. dev. 0.27 pN). A swimmer that separated from the glass surface and then reemerged gave apparent instantaneous forces up to ~17 pN. The wide range may be due to the variety in size and shape, as well as differences in speed close to and far from nearby surfaces. Similar to the standing behavior observed in ref. 1, we see that the swimmers are attracted to their own reflections and orient themselves perpendicular to the substrate for short amounts of time (Fig. 7B). But since the swimmers often quickly reorient, the attractive force must be small, likely very similar to the magnitude of the streaming propulsive force (~1–2 pN). Similarly, we note in Fig. 7C and ESI,† Video S3 that some bubbles are transiently attracted to each other, which is likely a manifestation of the secondary Bjerknes force between two real-space bubbles. This force is also likely of a similar magnitude to streaming propulsion. While transient in this case, these types of forces could lead to interesting types of global self-assembly and collective behavior if the ratio between streaming and Bjerknes forces could be tuned, opening up new opportunities in this area.

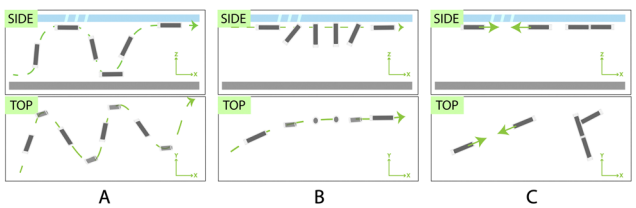

Fig. 7 (A) Rapid helical motion (B) linear motion with transient pauses due to attraction to the surfaces, (C) transient self-assembly of swimmers due to secondary Bjerknes forces.

In conclusion, we can fabricate microswimmers from the empty frustules of *Aulacoseira granulata*, which exhibit complex patterns of motion that derive from their cylindrical structure. Algae grow by efficiently converting nutrients in water, carbon dioxide from the air, and light energy and produce highly conserved cylindrical structures. As algal growth is inherently scalable, we envision that bulk quantities can be produced, characterized as active colloids, and potentially deployed in applications that require bulk quantities of powered swimmers. One can also imagine genetic engineering of diatoms to better cater their structures to obtain more predictable and well-behaved swimmers, and perhaps even create new types of self-assembled structures.

Author contributions

All authors contributed to the ideas and design of experiments for this project. Experimental work was carried out by M. C. O., and all authors discussed the data. M. C. O. drafted the manuscript, which was edited by T. E. M. and J. M. M.

Data availability

All original data are available upon request from the corresponding author.

Conflicts of interest

The authors have no conflicts of interest to declare.

Acknowledgements

We thank Owen Land (University of Pennsylvania) for lending a hydrophone and Mark Schafer and Peter Lewin (Drexel University) for their guidance regarding transducers and their inherent vibrational modes. M. C. O acknowledges support from the Molecular Life Sciences program at the University of Pennsylvania. This work was carried out in part at the Singh Center for Nanotechnology, which is supported by the NSF National Nanotechnology Coordinated Infrastructure Program under grant NNCI-2025608.

Notes and references

1 L. Ren, N. Nama, J. M. McNeill, F. Soto, Z. Yan, W. Liu, W. Wang, J. Wang and T. E. Mallouk, 3D Steerable, Acoustically Powered Microswimmers for Single-Particle Manipulation, *Sci. Adv.*, 2019, **5**(10), eaax3084, DOI: 10.1126/sciadv.aax3084.

2 J. M. McNeill and T. E. Mallouk, Acoustically Powered Nano- and Microswimmers: From Individual to Collective Behavior, *ACS Nanosci. Au*, 2023, **3**(6), 424–440, DOI: 10.1021/acsnanoscienceau.3c00038.

3 A. Ghosh and P. Fischer, Controlled Propulsion of Artificial Magnetic Nanostructured Propellers, *Nano Lett.*, 2009, **9**(6), 2243–2245, DOI: **10.1021/nl900186w**.
4 A. M. Brooks, M. Tasinkevych, S. Sabrina, D. Velegol, A. Sen and K. J. M. Bishop, Shape-Directed Rotation of Homogeneous Micromotors via Catalytic Self-Electrophoresis, *Nat. Commun.*, 2019, **10**(1), 495, DOI: **10.1038/s41467-019-08423-7**.
5 J. Palacci, S. Sacanna, A. Vatchinsky, P. M. Chaikin and D. J. Pine, Photoactivated Colloidal Dockers for Cargo Transportation, *J. Am. Chem. Soc.*, 2013, **135**(43), 15978–15981, DOI: **10.1021/ja406090s**.
6 E. L. Jewell, W. Wang and T. E. Mallouk, Catalytically Driven Assembly of Trisegmented Metallic Nanorods and Polystyrene Tracer Particles, *Soft Matter*, 2016, **12**(9), 2501–2504, DOI: **10.1039/C5SM03066H**.
7 R. J. Archer, A. J. Parnell, A. I. Campbell, J. R. Howse and S. J. Ebbens, A Pickering Emulsion Route to Swimming Active Janus Colloids, *Adv. Sci.*, 2018, **5**(2), 1700528, DOI: **10.1002/advs.201700528**.
8 S. Gangwal, A. Pawar, I. Kretzschmar and O. D. Velev, Programmed Assembly of Metallodielectric Patchy Particles in External AC Electric Fields, *Soft Matter*, 2010, **6**(7), 1413–1418, DOI: **10.1039/B925713F**.
9 J. Yan, M. Bloom, S. C. Bae, E. Luijten and S. Granick, Linking Synchronization to Self-Assembly Using Magnetic Janus Colloids, *Nature*, 2012, **491**(7425), 578–581, DOI: **10.1038/nature11619**.
10 S. Yang, Z. Tian, Z. Wang, J. Rufo, P. Li, J. Mai, J. Xia, H. Bachman, P.-H. Huang, M. Wu, C. Chen, L. P. Lee and T. J. Huang, Harmonic Acoustics for Dynamic and Selective Particle Manipulation, *Nat. Mater.*, 2022, **21**(5), 540–546, DOI: **10.1038/s41563-022-01210-8**.
11 Z. Wang, J. Rich, N. Hao, Y. Gu, C. Chen, S. Yang, P. Zhang and T. J. Huang, Acoustofluidics for Simultaneous Nanoparticle-Based Drug Loading and Exosome Encapsulation, *Microsyst. Nanoeng.*, 2022, **8**(1), 1–11, DOI: **10.1038/s41378-022-00374-2**.
12 Y. Deng, A. Paskert, Z. Zhang, R. Wittkowski and D. Ahmed, An Acoustically Controlled Helical Microrobot, *Sci. Adv.*, 2023, **9**(38), eadh5260, DOI: **10.1126/sciadv.adh5260**.
13 C. Dillinger, N. Nama and D. Ahmed, Ultrasound-Activated Ciliary Bands for Microrobotic Systems Inspired by Starfish, *Nat. Commun.*, 2021, **12**(1), 6455, DOI: **10.1038/s41467-021-26607-y**.
14 A. Del Campo Fonseca, C. Glück, J. Droux, Y. Ferry, C. Frei, S. Wegener, B. Weber, M. El Amki and D. Ahmed, Ultrasound Trapping and Navigation of Microrobots in the Mouse Brain Vasculature, *Nat. Commun.*, 2023, **14**(1), 5889, DOI: **10.1038/s41467-023-41557-3**.
15 A. Aghakhani, O. Yasa, P. Wrede and M. Sitti, Acoustically Powered Surface-Slipping Mobile Microrobots, *Proc. Natl. Acad. Sci. U. S. A.*, 2020, **117**(7), 3469–3477, DOI: **10.1073/pnas.1920099117**.
16 D. Ahmed, M. Lu, A. Nourhani, P. E. Lammert, Z. Stratton, H. S. Muddana, V. H. Crespi and T. J. Huang, Selectively Manipulable Acoustic-Powered Microswimmers, *Sci. Rep.*, 2015, **5**, 9744, DOI: **10.1038/srep09744**.
17 J. M. McNeill, N. Nama, J. M. Braxton and T. E. Mallouk, Wafer-Scale Fabrication of Micro- to Nanoscale Bubble Swimmers and Their Fast Autonomous Propulsion by Ultrasound, *ACS Nano*, 2020, **14**(6), 7520–7528, DOI: **10.1021/acsnano.0c03311**.
18 J. Rufo, F. Cai, J. Friend, M. Wiklund and T. J. Huang, Acoustofluidics for Biomedical Applications, *Nat. Rev. Methods Primers*, 2022, **2**(1), 1–21, DOI: **10.1038/s43586-022-00109-7**.
19 V. Iacovacci, E. Diller, D. Ahmed and A. Menciassi, Medical Microrobots, *Annu. Rev. Biomed. Eng.*, 2024, **26**, 561–591, DOI: **10.1146/annurev-bioeng-081523-033131**.
20 R. Ragni, S. R. Cicco, D. Vona and G. M. Farinola, Multiple Routes to Smart Nanostructured Materials from Diatom Microalgae: A Chemical Perspective, *Adv. Mater.*, 2018, **30**(19), e1704289, DOI: **10.1002/adma.201704289**.
21 N. Kröger, Prescribing Diatom Morphology: Toward Genetic Engineering of Biological Nanomaterials, *Curr. Opin. Chem. Biol.*, 2007, **11**(6), 662–669, DOI: **10.1016/j.cbpa.2007.10.009**.
22 Y. Seo, J. Leong, J. D. Park, Y.-T. Hong, S.-H. Chu, C. Park, D. H. Kim, Y.-H. Deng, V. Dushnov, J. Soh, S. Rogers, Y. Y. Yang and H. Kong, Diatom Microbubbler for Active Biofilm Removal in Confined Spaces, *ACS Appl. Mater. Interfaces*, 2018, **10**(42), 35685–35692, DOI: **10.1021/acsami.8b08643**.
23 Image Analyst. *How can I write code to calculate frames differnces of video frames*. **https://www.mathworks.com/matlabcentral/answers/168762-how-can-i-write-code-to-calculate-frames-differnces-of-video-frames?s_tid=srchtitle**.
24 R. Pruim and D. T. Kaplan, The Mosaic Package: Helping Students to ''Think with Data'' Using R, *R. J.*, 2017, **9**(1), 77–102.
25 J. Schindelin, I. Arganda-Carreras, E. Frise, V. Kaynig, M. Longair, T. Pietzsch, S. Preibisch, C. Rueden, S. Saalfeld, B. Schmid, J.-Y. Tinevez, D. J. White, V. Hartenstein, K. Eliceiri, P. Tomancak and A. Cardona, Fiji: An Open-Source Platform for Biological-Image Analysis, *Nat. Methods*, 2012, **9**(7), 676–682, DOI: **10.1038/nmeth.2019**.
26 N. Tarantino, J.-Y. Tinevez, E. F. Crowell, B. Boisson, R. Henriques, M. Mhlanga, F. Agou, A. Israël and E. Laplantine, TNF and IL-1 Exhibit Distinct Ubiquitin Requirements for Inducing NEMO–IKK Supramolecular Structures, *J. Cell Biol.*, 2014, **204**(2), 231–245, DOI: **10.1083/jcb.201307172**.
27 The MathWorks Inc. MATLAB Version: 23.2.0 (R2023b), 2023.
28 W. Wang, W. Duan, A. Sen and T. E. Mallouk, Catalytically Powered Dynamic Assembly of Rod-Shaped Nanomotors and Passive Tracer Particles, *Proc. Natl. Acad. Sci. U. S. A.*, 2013, **110**(44), 17744–17749, DOI: **10.1073/pnas.1311543110**.